

# INTERNATIONAL SOCIETY FOR SOIL MECHANICS AND GEOTECHNICAL ENGINEERING



*This paper was downloaded from the Online Library of the International Society for Soil Mechanics and Geotechnical Engineering (ISSMGE). The library is available here:*

<https://www.issmge.org/publications/online-library>

*This is an open-access database that archives thousands of papers published under the Auspices of the ISSMGE and maintained by the Innovation and Development Committee of ISSMGE.*

*The paper was published in the proceedings of the 20<sup>th</sup> International Conference on Soil Mechanics and Geotechnical Engineering and was edited by Mizanur Rahman and Mark Jaksa. The conference was held from May 1<sup>st</sup> to May 5<sup>th</sup> 2022 in Sydney, Australia.*

## Basic research on the resisting mechanism of the uplifting belled pile

Recherche fondamentale sur le mécanisme de résistance au soulèvement des pieux à base évasée

**Takatoshi Kiriya** & Yoshiharu Asaka

*Institute of Technology, Shimizu Corporation, Japan, kiriyama@shimz.co.jp*

Takumi Hirai

*Technology Development Section Engineering Division, Tokyo Soil Research Corporation, Japan*

**ABSTRACT:** In this study, observation experiments using centrifuge and PIV have been performed in order to understand belled pile shapes' effects on the resisting mechanism in uplift. The experiments have been performed using several kinds of piles with different belled angles. The load-displacement curves at the pile head were monitored, and digital images of ground deformations from the side were captured for PIV image analysis. By relating the load-displacement curves and the imaged ground deformation by PIV, it is revealed that the shear strain distributes in bulb-shaped repeatedly as the vertical load increase, resulting in that these repeated bulb domains resist the uplifting load. The numerical simulation to reproduce the experimental results has been constructed to understand the ground behavior and simulate the ultimate failure mode when belled piles are completely uplifted. The simulation demonstrated that the ultimate failure mode of belled piles shows the cylinder-shaped failure mode. Both experiments and numerical analyses reveal the resisting mechanism; the resisting ground generates a bulb-shaped domain at first, and the belled piles are completely pulled out with cylinder-shaped failure mode after.

**RÉSUMÉ :** Dans la présente étude, des expériences d'observation ayant recours à la centrifugation et la vélocimétrie par images de particules (VIP) ont été réalisées afin de comprendre les impacts des formes des pieux à base évasée sur le mécanisme de résistance au soulèvement. Les courbes charge-déplacement à la tête des pieux étaient surveillées, et des images numériques des déformations du sol du côté ont été capturées pour l'analyse des images VIP. En reliant les courbes charge-déplacement et les images des déformations du sol par VIP, il s'avère que la déformation de cisaillement se répartit de façon répétée en forme de bulbe à mesure que la charge verticale augmente, ce qui a pour effet que ces domaines répétitifs en forme de bulbe résistent à la charge de soulèvement. La simulation numérique pour reproduire les résultats expérimentaux a été construite pour comprendre le comportement du sol et simuler le mode de défaillance ultime lorsque les pieux à base évasée sont soulevés. Les expériences et les analyses numériques révèlent les unes comme les autres le mécanisme de résistance, à savoir que le sol résistant provoque d'abord un domaine en forme de bulbe, et les pieux à base évasée sont ensuite entièrement extraits en mode de défaillance des formes cylindriques.

**KEYWORDS:** belled pile, uplift resistance, centrifuge test, PIV, numerical simulation

### 1 INTRODUCTION.

The burden on pile foundations has been increasing over time as structures have become higher and building frames have increased in span. The uplift burden has also been rising due to the rocking effect of high-rise buildings, especially when they suffer from wind and earthquakes. Although a belled pile is expected to offer resistance to uplift while reducing material consumption and being easier on the environment, the uplift resistance of belled piles has not been studied from a geotechnical point of view and the mechanism of uplift resistance remains unclear.

To evaluate the uplift resistance of belled piles, we need to investigate how earth pressure acts on the pile bell and reveal the resistance mechanism. In this regard, the authors have been pursuing centrifuge-based experimental studies and numerical simulations of belled piles in uplift (e.g. Kiriya et al., 2020).

This paper reports on observations from centrifuge experiments and the results of numerical simulations. In the centrifuge experiments, observations are made by capturing digital images of uplifting piles through an observation window on the side of a semi-cylinder soil box. After capture, the digital images are analyzed by particle image velocimetry (PIV) and the displacement and shear strain distributions within the ground are visualized, revealing how resisting earth pressure acts on the pile during uplift. Additionally a numerical method applicable to belled pile uplift is developed and used to simulate the ultimate behavior of uplifted belled piles.

### 2 CENTRIFUGE MODELING

The experiment to observe ground behavior around a belled pile during uplift was carried out in a centrifuge apparatus under a centrifugal gravity of 60(G). This means that the physical pile models were scaled at 1/60 size. However, sizes and physical properties are given in this paper at prototype scale.

The soil box used in the experiments was semi-cylindrical in shape and had an observation window on the flat side. The cylinder was 30 m in diameter and 30 m in height. Figure 1 shows the model piles. The three belled pile designs all have shaft and bell diameters of 1.2 m and 3 m, respectively, while the bell angle is varied: 10°, 20°, and 30°. The model piles were cut in half vertically, to allow placement against the observation window. Since these were models of cast-in-place piles, their surface was finished with sand to provide appropriate skin friction. The cut surface placed against the observation window was prepared with a three-layered interface to reduce friction: on layer of polyurethane sheet attached directly to the cut surface, then another layer of polyethylene sheet with a film of oil in between.

Toyoura sand ( $\rho_s=2.65$  g/cm<sup>3</sup>,  $\rho_{max}=1.65$  g/cm<sup>3</sup>,  $\rho_{min}=1.34$  g/cm<sup>3</sup>), with relative density ( $D_r$ ) over 90%, was used as the model ground geomaterial. The model ground was prepared by the air pluviation method using a sand hopper over the sand box. The ground was prepared in two steps. In the first step, the base ground was prepared to a thickness of 12 m (200 mm in the model). At this point, the pile was placed on the base ground,

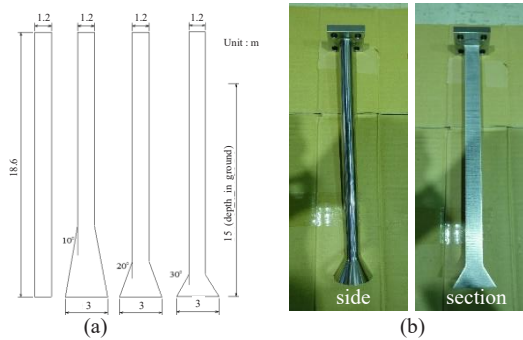


Figure 1. Model piles for observational experiments. (a) Shaft and bottom diameters are 1.2 m and 3 m respectively, and bell angles are 10°, 20°, and 30°. (b) Piles are cut in half and coated with sand. A three-layers interface of polyurethane-polyethylene-oil reduces friction where the pile is in contact with the observation window.

with the pile head secured to the sand box frame. At this same pile depth, a bender element was installed to monitor the ground shear velocity. In the second step, the surface ground was added to a thickness of 15 m. This two-step procedure simulates the construction of cast-in-place piles, in which piles are installed after ground excavation.

Photo 1 shows the physical model mounted on the centrifuge. The pile head is fixed to the vertical jack (maximum load and stroke: 180 MN and 60 cm, respectively) on the centrifuge platform. The vertical load and displacement at the pile head are monitored with a load cell and a laser displacement meter.

Loading was controlled by displacement with a loading rate of 0.2 mm/min. During loading, digital images were captured from the side of the sand box with the digital camera. The digital camera was fixed 60 cm away from the observation window by the steel frame, with images captured automatically every 5 seconds. In order to avoid reflections from the observation window, the centrifuge pit was kept in dark, and the observation window was made to glow with disperse light using LEDs.

### 3 PARTICLE IMAGE VELOCIMETRY

Particle image velocimetry (PIV) is an imaging technique that enables relative deformations in solid mechanics to be traced by comparing brightness in two digital images. The digital images captured in the centrifugal experiment are processed by PIV to visualize ground deformation as the belled piles are uplifted.

The PIV analysis procedure is as follows:

- step1: Convert images to grayscale
- step2: Relocate images to maintain a fixed point at the same position
- step3: Exclude blackened piles from image tracing
- step4: Obtain displacements using PIV technique
- step5: Calculate maximum shear strain from displacements

Here, displacement refers to the relative displacement as compared with the initial image before loading. The PIV analysis

Table 1. PIV analysis conditions

Item	Value
Method	FFT Grid Interlogation
Image size	1600 x 1800 (pixel)
Cell size	8 x 8 (pixel)
Phase	3
Disp.	Relative displacement from initial image

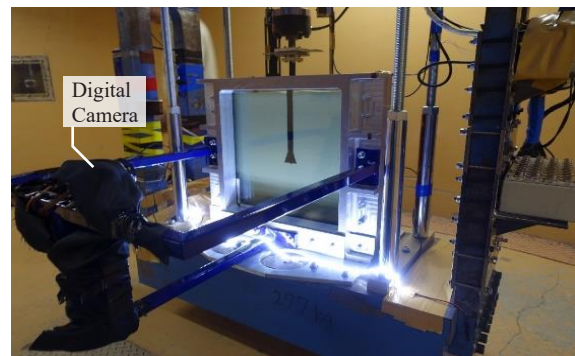


Photo 1. The digital camera is secured at a distance from the observation window and covered with a black cloth to prevent reflection on the window. Digital images are captured every 5 seconds while under 60 (G) centrifugal force.

conditions are listed in Table 1. An 8 x 8 pixel tracing window is selected, which is equivalent to 1 x 1 mm in model scale. To reduce the computational cost of particle tracing, a multi-window tracing method (three phases) is employed.

### 4 OBSERVATIONS AND PIV RESULTS

#### 4.1 Observation of ground behavior under belled piles during uplift

Figure 2 shows relationship between uplift resistance (load) and pile head uplift (displacement) at the pile head for the 20° belled pile during uplift, where uplift resistance excludes the self-weight of the pile. This load-displacement curve exhibits three distinct phases. Phase-I (from origin to point [b] in Figure 2) is the elastic-plastic zone, in which the ground initially exhibits elastic behavior and then plastic behavior. Phase-II (from point [b] to point [b'] in Figure 2) is the sliding zone, in which the first shear band is fully mobilized. In this phase, there is no increase in resistance in the load-displacement relationship, meaning that deformation occurs along a localized shear zone, where a slip line forms. It is noted that, in this phase, friction between the sectioned pile and the observation window may evolve from static to dynamic. A load-displacement relationship obtained from a full cylinder sand box test does not exhibit this behavior, so it is likely that friction against the observation window induced its emergence. Phase-III (point [b'] and beyond) is the zone in which the yield surface expands into the surrounding area, meaning another shear band initiates a new localized zone once the inner shear band is fully localized. In this phase, the load-displacement relationship shows a gradual increase in resistance again, corresponding to the increased yield surface around the belled part of the pile.

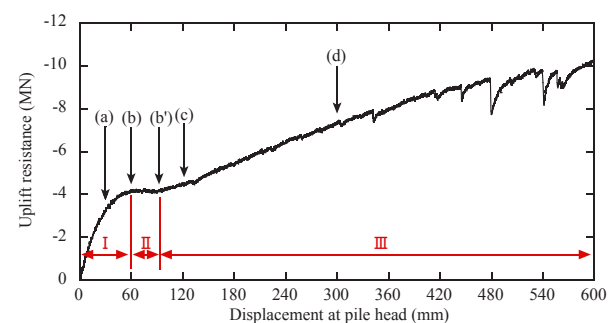


Figure 2. Load-displacement relationship of 20 degree Belled pile in uplift. The relationship is divided into three phases; I: the load show gradual increase; II: the friction between pile section and the observation window was sliding; III: the yield surface expanded inducing the increase of uplift resistance.

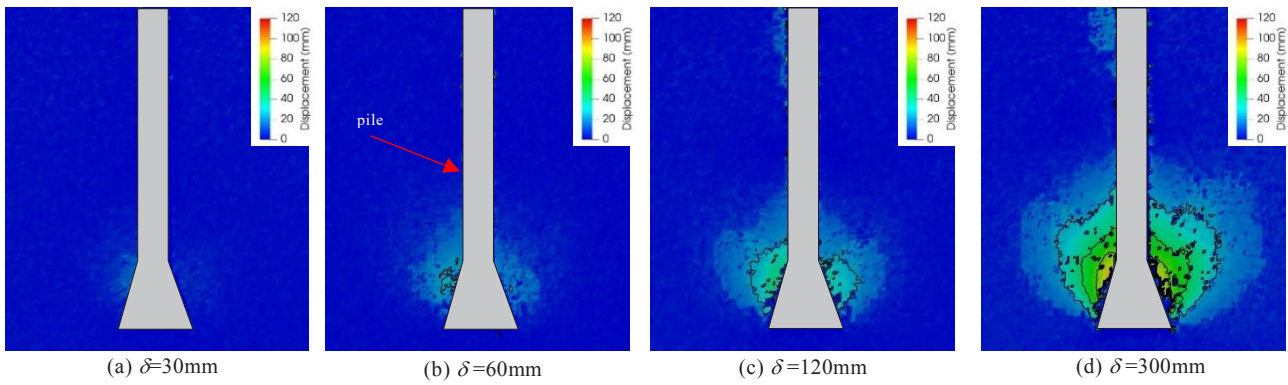


Figure 3. Total ground displacement in 20° belled pile uplift. ( $\delta$ : pile head uplift)

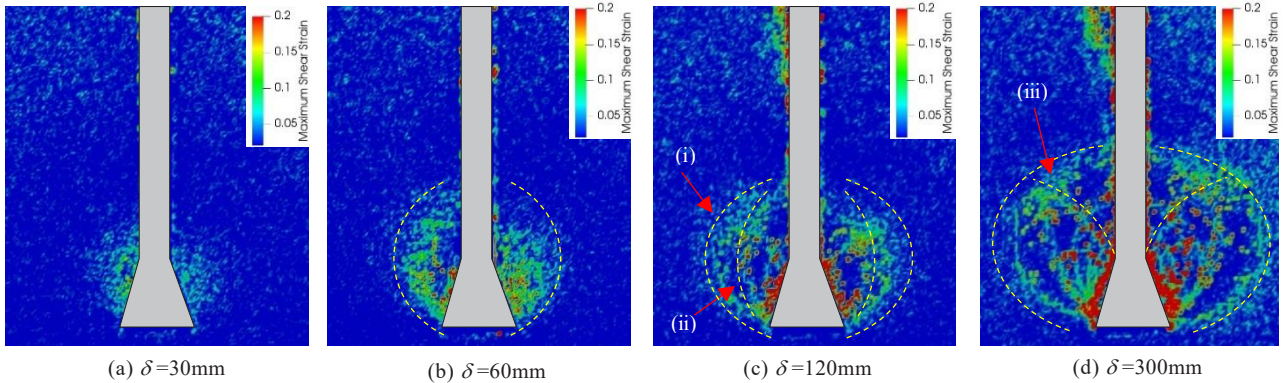


Figure 4. Ground maximum shear strain in 20° belled pile uplift. ( $\delta$ : pile head uplift). (a) with 30mm uplift no shear strain localization is seen. (b) with 60mm uplift there is a clear shear strain localization zone shaped like a bulb around the bell. (c) with 120mm uplift a second bulb appears outside the first. (d) with 300mm uplift there are repeated bulb shapes around the bell and a conjugated shear localization zone curving outward from the top of bell.

Figures 3 and 4 show the total ground displacement and maximum shear strain, respectively. Each contour line in Figure 3 represents 24 mm of displacement. Let us consider the load-displacement relationship again, in relation to the ground responses shown in Figures 3 and 4. The ground at 30 mm of uplift, Figure 4(a), shows no clear localized shear zone. Although ground behavior may be plastic, there is no evidence of shear localization in any part of the ground. At 60 mm of uplift, Figure 4(b), the first localized shear zone appears in a bulb shape around the belled part of the pile. Then at 120 mm of uplift, Figure 4(c), a second localized shear zone appears (ii) outside the first bulb (i). This means the ground zone resisting the uplift force is expanding as the external load increases. The ground at 300 mm of uplift, Figure 4(d), has concentric localized shear zones in bulb shapes. These repeated bulbs correspond to the increased uplift force. The ground also exhibits a conjugated shear band (iii) outward from the top of the belled part of the pile.

Kanatani et al. (1973) performed experiments under 1G conditions and observed a slip line. This slip line corresponds to the shear strain in Figure 4(d)-(iii), which is conjugated with the bulb-shaped shear regions. These two sets of observations at 1G and 60G differ in soil conditions, such as confining pressure and geomaterial, as well as in experimental setup. (That is, the confining pressure is relatively low under 1G while it is equivalent to an actual pressure in a centrifuge; the ground dilates more readily at 1G while dilatation is inhibited at actual confining pressures. An even earlier study also pointed out that these ground conditions affect ground deformation after loading (Vesic, 1963).

#### 4.2 Comparison among belled piles with different bell angles

In order to investigate the effect of bell angle on uplift resistance, three piles with angles of 10°, 20°, and 30° were tested as explained in section 2. Figure 5 shows the load-displacement relationships for these three different angled piles. All three load-

displacement relationships show an initial gradual increase (until displacement reaches 60 mm for the 10° and 20° piles and 120 mm for the 30° pile). The load is then constant for a time, and then uplift resistance begins to increase again. Figures 6 and 7 show the maximum shear strain and total displacement for the three different angled piles. The maximum shear strain is shown at the three displacements numbered (1), (2), and (3) in Figure 5.

Focusing on the resisting domain in each case, which is recognizable as the outermost bulb shape (slip line) around each belled pile, it measures 0.6D (horizontal) x 2.3D (vertical) in the 10° case at 60 mm of uplift, 0.5D x 1.8D in the 20° case, and 0.5D x 1.7D in the 30° case (where D represents the base diameter of the belled pile). That is, the resisting domain has a horizontal range 0.5D-0.6D from the toe of the bell while the vertical range is 1.7D-2.3D from the bottom of the pile. The vertical extent of the resisting domain increases as the bell angle becomes smaller.

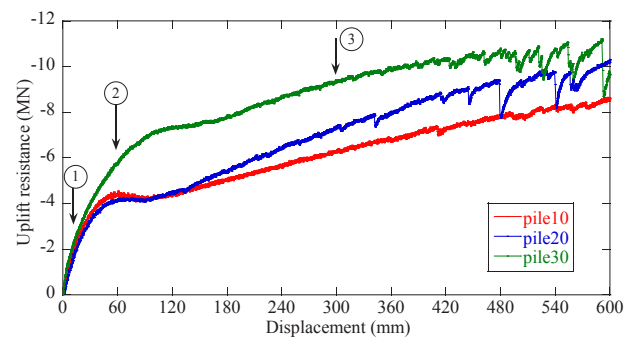


Figure 5. Comparison of load-displacement relationship among difference belled angles. Initial stiffness is almost the same regardless of belled angles. The uplift resistance of each pile is in order of 30, 20, 10 degree. The uplift resistance depends on belled angle

These domains increase in width and height as the piles are uplifted further, e.g., 0.9D x 2.4D in the 10° case; 1.0D x 2.2D in the 20° case; and 1.3D x 2.4D in the 30° case. The range of resisting domain horizontal extent is 0.9D-1.3D at 300 mm of uplift, with the resisting domain becoming wider at a larger bell angle. The vertical range of the resisting domain at this uplift is 2.2-2.4D. In this dense sand, the domain of influence more readily widens in the horizontal direction than in the vertical direction.

## 5 NUMERICAL SIMULATION OF ULTIMATE FAILURE MODE OF BELLED PILE IN UPLIFT

The centrifugal experiment was simulated numerically in order to assess the ultimate failure mode of belled piles in uplift. The following sections detail the numerical procedure, simulation conditions, and results.

### 5.1 Numerical method for large deformations

A numerical method based on the material point method (MPM) was employed to assess the ultimate failure mode of belled piles at the point of full uplift. The arbitrary particle domain interpolation (APDI) method (Kiryama and Higo, 2020) reported by the authors in the literature was used.

Geomaterial deformation is characterized by strain localization, which is quite difficult to model using mesh-based simulation methods because mesh tangling readily occurs when the material undergoes large deformations. Particle-based methods are capable of analyzing large deformations without the problem of mesh tangling because they are free from node connectivity. On the other hand, particle-based methods have a higher computing cost when applied to practical simulations. The APDI method combines particles and elements in the same simulation by using a numerical grid. The method enables us to model large deformations with high spatial resolution, while reducing computational cost at the same time.

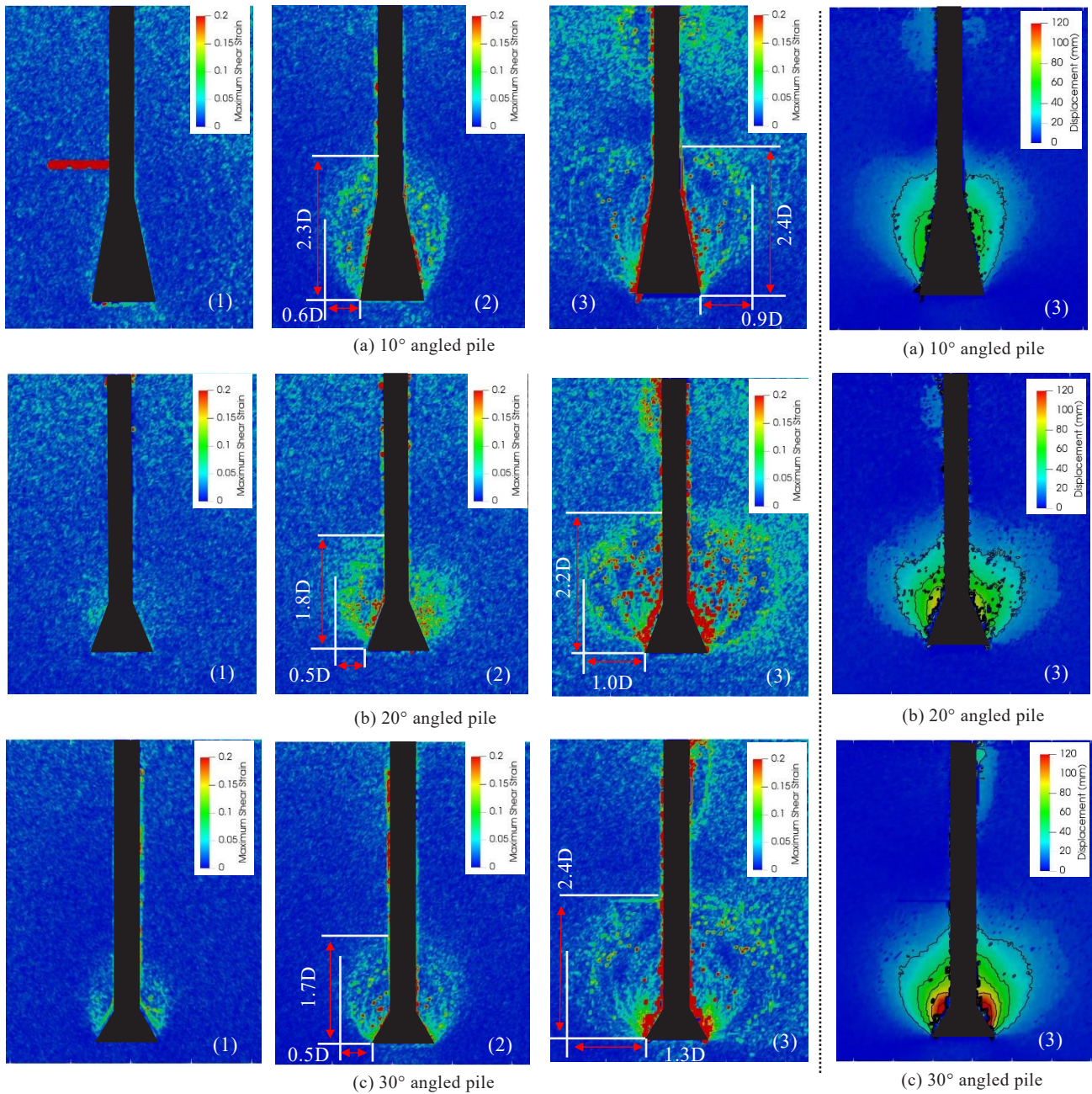


Figure 6. Maximum shear strain (displacement at pile head): (1)  $\delta=12$ mm, (2)  $\delta=60$ mm, (3)  $\delta=300$ mm

Figure 7. Total displacement at (3)  $\delta=300$ mm in Figure 5-

### 5.2 Numerical conditions for simulation of belled pile in uplift

Figure 8 shows the numerical models of piles with different bell angles in uplift. These models replicate the experiments, using a cylindrical sand box of the same size as described in previous sections, but in this case modeled as a full cylinder. The pile and the sand box are axisymmetric shaped, so a 2D axisymmetric formulation was employed for the simulation. In the numerical model, ground in the vicinity of the piles is modeled using particles, because large deformations are expected in this region. The piles themselves and the surrounding ground are modeled using elements, since deformation is expected to be small. Both sides of the model are horizontally fixed, and the bottom is fixed. The material properties of the piles and ground are listed in Table 2. Young's modulus of the sand is estimated from measured shear velocity, as monitored by the bender element: 100 m/s under 1G and 250 m/s under 60G. The internal friction angle is estimated from previous research. Pile density in the simulations is adjusted to match the total weight that actual piles would have, because the numerical (solid) and experimental (pipe-shaped with attachments) piles differ from each other. Young's modulus of the piles is set such that they are relatively rigid compared with ground stiffness.

Table 2. Material property for geomaterial and pile

	$\gamma$ (kN/m <sup>3</sup> )	$E$ (kN/m <sup>2</sup> )	$\nu$ (-)	$\alpha$ (deg.)	$\phi$ (deg.)
Toyoura sand	16.0	119000	0.3	-	43
pile 10 deg.	89.8	1.0e8	0.3	10	-
pile 20 deg.	93.7	1.0e8	0.3	20	-
pile 30 deg.	95.9	1.0e8	0.3	30	-

$\gamma$ : average unit weight,  $E$ : Young's modulus,  $\nu$ : Poisson's ratio,  $\alpha$ : inclined angle,  $\phi$ : internal friction angle.

### 5.3 Belled pile ultimate failure mode in uplift

It should be noted again that we used two types of soil boxes; one is a cylinder soil box for measurements; the other is a semi-cylinder soil box, which is a half cut of a cylinder soil box in photo 1, for observation. The experimental result below were obtained from another series of centrifuge tests, in which a cylinder soil box was used. Figure 9 compares load-displacement relationships at the pile head between the experimental and numerical results. Uplift displacement is standardized by dividing by bottom diameter. The experimental and numerical results agree well with each other up to  $\delta/D=0.04$  whatever the

bell angle. Thereafter, the analytical results indicate a slower increase in uplift resistance. The experimental results peak at around  $\delta/D=0.12$  before falling gradually, while the simulation shows a constantly rising uplift resistance. The numerical results do not peak because the loading condition at pile head is defined not in terms of particle displacements but by the application of load. In the numerical simulation, when the geomaterial reaches a yield surface, it deforms rapidly and is uplifted in a moment, taking the nearby ground with it.

Figures 10-12 show the numerical results of maximum shear strain and total displacement for the 10°, 20°, and 30° belled piles. There are three concentrations of shear strain, as indicated in Figure 11(a): s1 is along the pile shaft; s2 is vertical from the toe of the bell; and s3 is outward from the toe of the bell. Concentration s3 seems to correspond to the first bulb as visualized in the PIV observational experiment. Before full uplift of the piles (Figures 10-12 (a)), this bulb reaches a greater height as the bell angle becomes smaller, which agrees with the PIV observations. At full uplift, the piles carry with them the soil immediately above the bell, resulting in a cylinder-shaped resistance domain with any bell angle.

## 6 CONCLUSIONS

Belled piles with three different bell angles are subjected to uplift in observational experiments with PIV image analysis and numerical simulations of piles are also implemented. The following findings are revealed by this work.

- i) During pile uplift, repeated bulb-shaped slip lines are observed in the ground.
- ii) The horizontal width of the bulb that is seen to form around the belled part increases with bell angle.
- iii) The bulb around the 10° belled pile reaches higher than that around the 20° and 30° belled piles.
- iv) The numerical simulation demonstrates that, in uplift, a bulb-shaped region of ground around a belled pile resists the uplift force until the point of full uplift, while the resistance region is cylinder-shaped when the belled piles reach full uplift.

## 7 REFERENCES

- Kanatani, Y., Sato, H., and Akino, N., 1973, Mokeikiso no hikinuki jikken oyobi kaiseki, Proceedings of 8<sup>th</sup> annual conference of Japanese Geotechnical Society, 439-442. (in Japanese)  
 Kanatani, Y., Sato, H., Akino, N., and Okumura, K., 1975, Mokeikiso no hikinuki jikken oyobi kaiseki (report no.2), Proceedings of 10<sup>th</sup>

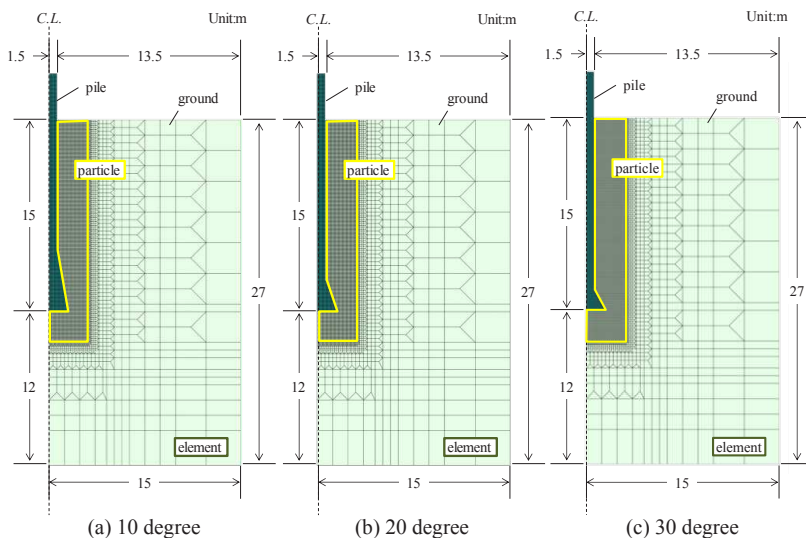


Figure 8. Numerical models for belled piles and surrounding ground (prototype)

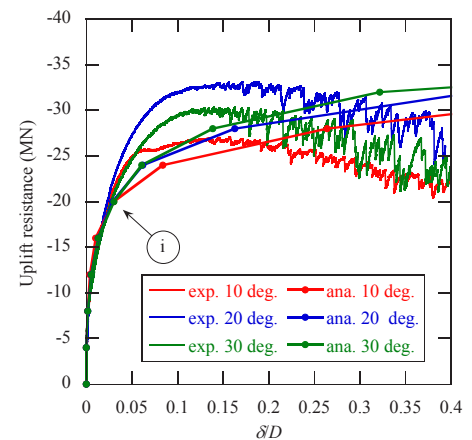


Figure 9. Load-displacement relationship at pile head. ( $\delta$ : uplift,  $D$ : bottom diameter)

annual conference of Japanese Geotechnical Society, 455-458. (in Japanese)

Kiriyama, T. and Higo, Y., 2020, Arbitrary Particle Domain Interpolation Method and Application to Problems of Geomaterial Deformation, *Soils and Foundations*, Vol.60, No.6, 1422-1439.

Kiriyama, T., Hirai, T., and Iwai, T., 2020, Basic research on supporting mechanism of uplifting belled pile: Part 1 Centrifugal experiment and image analysis. Proceedings of annual conference of Japanese Geotechnical Society. (in Japanese)

Vesic, A. S., 1963, Bearing capacity of deep foundations in sand, Highway Research Board Record, No.39.

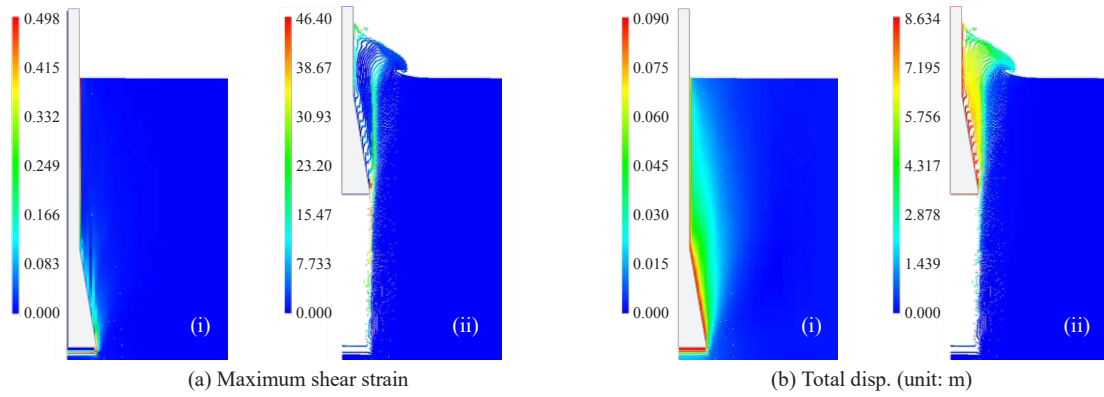


Figure 10. Numerical results for 10° angled pile (uplift force: (i) 20MN, (ii) 36(MN))

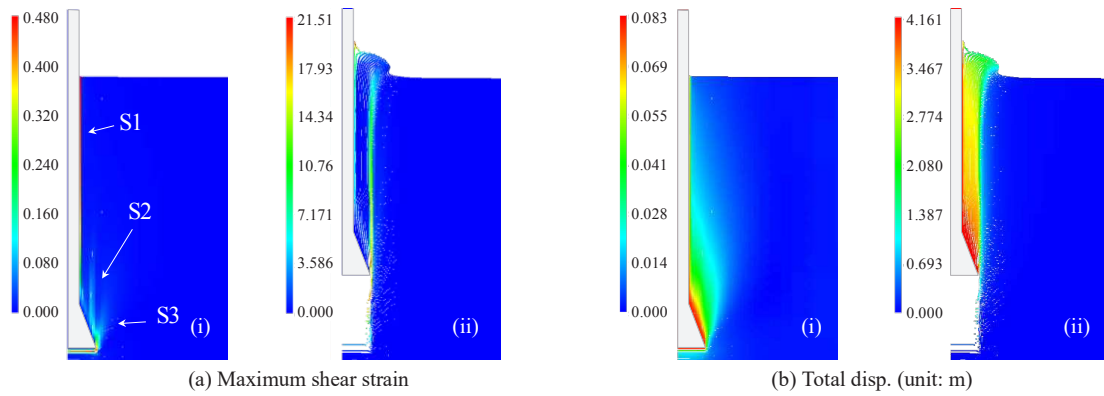


Figure 11. Numerical results for 20° angled pile (uplift force: (i) 20MN, (ii) 36(MN))

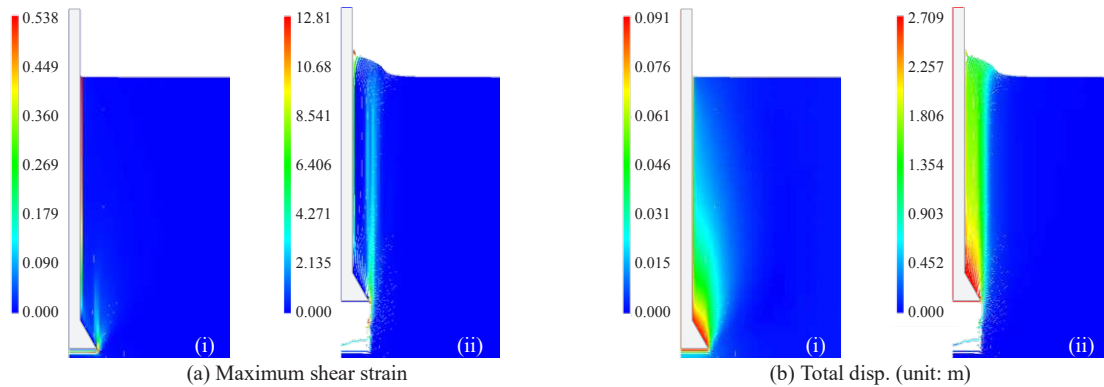


Figure 12. Numerical results for 30° angled pile (uplift force: (i) 20MN, (ii) 36(MN))